Modeling Chondrocyte Patterns by Elliptical Cluster Processes

Martin Meinhardt[a*], Sebastian Lück[a*], Pascal Martin[b], Tino Felka[b], Wilhelm Aicher[c], Bernd Rolauffs[b†], Volker Schmidt[a]

[a]Institute of Stochastics, Ulm University, Germany
[b]BG Trauma Center, Eberhard Karls University Tübingen, Germany
[c]Department of Orthopaedic Surgery, Eberhard Karls University Tübingen, Germany

* These authors contributed equally to this manuscript.

† Corresponding author:

BG Trauma Center
Eberhard Karls University Tübingen
Schnarrenbergstr. 95
D-72076 Tübingen
E-mail: berndrolauffs@googlemail.com
Phone: +49 7071 298 1120, Fax: +49 7071 29 4637

Short Title: Modeling Chondrocyte Patterns by Cluster Processes

Subject Categories: Image Classification, Image Processing, Bone/Cartilage, Quantitative Techniques, Fluorescence Microscopy

Abstract

Superficial zone chondrocytes (CHs) of human joints are spatially organized in distinct horizontal patterns. Among other factors, the type of spatial CH organization within a given articular surface depends on whether the cartilage has been derived from an intact joint or the joint is affected by osteoarthritis (OA). Furthermore, specific variations of the type of spatial organization are associated with particular states of OA. This association may prove relevant for early disease recognition based on a quantitative structural characterization of CH patterns. Therefore, we present a point process model describing the distinct morphology of CH patterns within the articular surface of intact human cartilage. This reference model for intact CH organization can be seen as a first step towards a model-based statistical diagnostic tool. Model parameters are fitted to fluorescence microscopy data by a novel statistical methodology utilizing tools from cluster and principal component analysis. This way, the complex morphology of surface CH patters is represented by a relatively small number of model parameters. We validate the point process model by comparing biologically relevant structural characteristics between the fitted model and data derived from photomicrographs of the human articular surface using techniques from spatial statistics.

Keywords : Chondrocyte, Cluster Analysis, Elliptical Cluster Process, Human Articular Cartilage, Knee Joint, Matérn Hardcore Process, Principal Component Analysis, Spatial Organization

1. Introduction

Articular cartilage is a connective tissue that functions hydrodynamically to bear loads and provide almost friction-free movement of diarthrodial joints (Kuettner et al. (1991)). It is composed of an extracellular matrix and sparsely distributed cells, the chondrocytes (CHs), which maintain matrix homeostasis via a synchronized balance between anabolism and catabolism (Kuettner et al. (1991); Poole (1997)). The organization of the CHs exhibits a depth-dependent density variation (Jadin et al. (2005)) on which the classification into superficial (0-10% tissue depth), middle (10-40%), and deep (40-100%) cartilage zones with distinct compositions, structures, and functions is based (Hunziker (1992)). In the deeper zones, the cell density is very low, and CHs are arranged in vertical columns (Stockwell and Meachim (1979)). In strong contrast, the superficial zone cell density is relatively high and CHs are arranged horizontally in groups at the articular surface (Stockwell and Meachim (1979)).
As published recently in this journal, human CHs of the superficial zone form distinct, almost planar patterns with various types of horizontally oriented clusters such as strings, round or oval clusters, pairs, and single CHs (Rolauffs et al. (2008); Schumacher et al. (2002)) (see Fig. 1, 2). Moreover, each articular joint surface was shown to be dominated by only one of these four patterns. Their presence within a specific articular surface correlated with the anatomical joint type suggesting a functional role of the organizational structure of superficial CHs (Rolauffs et al. (2008)). However, because functional roles of joint-specific CH patterns in the transverse plane have not been shown, alternative hypotheses e.g. that patterns are non-functional consequences of joint-specific developmental processes should also be mentioned. The

correlation of specific CH patterns with specific joint types (convex/concave, rotational, uni- or bi-axial joints) was uncovered in intact, healthy human joints. In joints affected by osteoarthritis (OA), a degenerative joint disease associated with loss of CHs and matrix elements, the spatial structure of CH patterns differed greatly from that of intact joints (Rolauffs et al. (2010, 2011)). This is partially due to recently unraveled spatial re-modeling processes, partially to unordered proliferation, and partially due to cell death. Thus, the type of cellular organizational structure that is present within a given articular surface is specific for the state of disease of the corresponding joint. This may likely prove relevant for the development of quantitative diagnostic methods in the context of both clinical and fundamental research.

This vision motivated us to describe the organizational structure of human superficial CHs by a mathematical point process model. In the present study we specifically address the intact surfaces of healthy joints and hypothesize that the spatial structure of the corresponding CH patterns can be characterized by a suitably constructed point process model. Consequently, this study aims to develop such a point process, which may in future work represent a reference model for the statistical comparison of microscopy data needing classification with respect to its degree of disease. Furthermore, we aim to evaluate the quality of model fit by a comparison of geometric characteristics of simulated realizations to those of real data. Our model characterizes CH patterns within the surface of intact cartilage by a relatively small set of model parameters, thus yielding a concise representation of the complex morphology. For a future statistical classification of CH patterns, a model-based approach offers

the advantage that arbitrarily large samples of reference images may be easily produced by computer simulation, whereas alternative bootstrap methods require large sets of experimental data. Large samples of virtual CH patterns which are structurally similar to real microscopy data are e.g. the basis for various Monte-Carlo tests comparing patient data to a reference model for intact cartilage.

The organizational structure of CHs is characterized by highly variable shapes of CH clusters (Rolauffs et al. (2008) and (2011)). The coexistence of different shapes such as strings and elliptical clusters in single microscopy images (Fig. 2) induced a need for a rather flexible cluster point process model to adequately capture morphological variability in intact cartilage. Thus, we suggest to model the occurring cluster shapes by non-overlapping random ellipses whose shape distribution can be fitted to a given dataset by variation of model parameters. This approach turns out to be well-suited to describe and reproduce the high variability of the CH patterns of intact cartilage.

2. Materials and methods for data acquisition

The articular cartilage data to be modeled in this study was obtained with institutional approval from healthy adult human tissue donors (n = 2, age 52 and 60 years) within 24 hours after death through the Gift of Hope Organ and Tissue Donor Network (Illinois, USA) and through the Institute of Pathology (n = 2, age 18 and 78 years), Eberhard Karls University (Tübingen, Germany). We investigated cartilage samples (n = 4) from a standardized location (medial condyle of the distal femur of the knee-joint in full joint extension) where they were taken from the superficial zone of the weight-bearing area of the articular surface and were stained with an immunofluorescent reagent as previously described in Rolauffs et al. (2008). Based

on these 4 cartilage samples, we recorded 8 images of the articular surface for our analysis. Prior to cartilage sample removal, the joints were graded according to a 5-point scale by a modified Collins grading (Muehleman et al. (1997)), using the following criteria: grade 0 (normal cartilage without signs of degeneration), grade 1 (minor surface roughening), grade 2 (fibrillations and fissuring), grade 3 (full defects covering less than 30% of the articular surface), and grade 4 (full defects covering more than 30% of the articular surface). Only joints with the grades 0-1 were included into this study. No other pathology than articular degeneration was observed in any of the joints. In brief, samples were washed (1% Triton X-100 in phosphate buffered saline (PBS)) for 5 min, stained for 60 min with propidium iodide (10μg/ml in PBS) and washed for 10 min with Tris-buffered saline (0.1M Tris, 0.15M NaCl, pH7.5). The superficial CH organization was visualized by fluorescence microscopy. Avoiding sectioning, all samples were viewed with a perpendicular angle between the optical axis of the microscope and the articular surface of the sample, providing a top-down view as described in Rolauffs et al. (2008), Rolauffs et al. (2010), and Rolauffs et al. (2011). The images were digitally recorded beneath the surface when CHs first came into focus (Illinois samples: Nikon Eclipse TE200 microscope at 10x magnification, objective Nikon Plan Fluor 10x/0.3 DIC L/N1, fluorescence filter appropriate for propidium iodide, manual exposure correction avoiding overexposed image areas, image resolution 696x520 pixels; Tübingen samples: Zeiss Axiophot at 10x magnification, objective EC Plan-Neofluar 10x/0.3 M27, fluorescence filter appropriate for propidium iodide, manual exposure correction avoiding overexposed image areas, image resolution 1388x1040 pixels). The CH positions were defined by

their Cartesian coordinates. In brief, each image was exported with Adobe Photoshop (San Jose, CA) into ImageJ (NIH, USA), converted into grayscale values, and analyzed by finding the maxima of the local grayscale values.

Thus, each CH nucleus was identified by its local grayscale maximum and marked with a single black pixel using the ImageJ function "find maxima" (output type"single points"), and an appropriate noise tolerance in combination with the "preview point selection". Because the analyzed CHs were mainly localized in the top optical plane, they were largely represented by crisp signals that were well suited for this type of image analysis. Cells with slightly blurred signals due to a slightly deeper z-axis position - did not represent a problem for this method. However, cell clusters rarely contained cells in and out of focus. In contrast, the signals of cells that were situated in a much deeper optical plane were blurred to such an extent that they were not analyzable by the presented method and were excluded from this study. The Cartesian coordinates of each CH nucleus center were determined with ImageJ using the method "Save xy coordinates".

The data to be modeled consisted of 8 images showing the positions of CH nuclei at the cartilage surface as found in the knee-joint (Fig. 2, left, and supplementary material). Image sizes and the numbers of contained CHs can be found in Tab. 1.

Due to the known physical dimensions of CHs in situ (Choi et al. (2007)), cell-cell distances smaller than $7.5\mu m$ were considered as artifacts (approximately 3% of all occurring cell-cell distances). Thus, of two points situated nearer than $7.5\mu m$ one point was randomly chosen and removed (1.1% to 3.4% of all points from each point pattern were removed). Consequently all remaining points kept an interpoint-

distance of at least $r = 7.5\mu m$. In point process theory, this distance is called a hardcore radius. If r was chosen smaller than $7.5\mu m$, differences in the cleaned data were marginal. For $r \geq 7.8\mu m$, a substantial number of points would have been removed from the data indicating that $7.5\mu m$ is a natural choice of the minimal inter-point-distance.

3. Results

3.1. Modeling concept

The nature of CH patterns requires a suitable point process model to satisfy the following properties.

(i) Clusters are non-overlapping and mostly well-separated.

(ii) Cluster shapes can be both string-like or elliptical.

(iii) Since surface CHs do not overlap, there is a hardcore distance of points (points closer to each other than this distance do not occur).

In order to construct a point process model with these features, we apply the following general approach which will be detailed in Section 3.3. Cluster centers are given by an *elliptical Matérn hardcore process*. This point process is characterized by the property that each point is surrounded by an ellipse of random axis lengths and orientation, where the ellipses are non-overlapping. In our model each of the ellipses contains itself a collection of so-called child points. This way the model achieves a clustered structure of the overall point pattern (Fig. 2). The required variability of cluster shapes ranging from string-like to circular patterns is induced

by an appropriate joint distribution for the axis lengths of the ellipses. The random child points in the ellipses are finally combined with a background point pattern outside the ellipses accounting for pairs and single CHs. The hardcore distance observed in the data is ensured by the choice of corresponding models for the child and background point processes (see Section 3.3).

3.2. Estimation of cluster shape parameters from the microscopy data

If a point process model is intended to describe a set of data, a fitting methodology for the model parameters needs to be established. For the point process introduced below, our attempts to fit the model by the widely used minimum contrast method (see e.g. Heinrich (1992); Illian et al. (2008); Stoyan (1992)) did not result in a satisfactory resemblance of cluster shapes between model and data. As a remedy, we developed a novel approach to fit the point process to our data based on a direct estimation of the ellipse shape distribution from the microscopy images. In the current section we derive and discuss this novel approach to identify ellipses based on point patterns restricted to the ellipse area.

In a first step we extracted CH clusters directly from the image data by a standard hierarchical cluster analysis using the single linkage method (see e.g. Arabie et al. (1996); Jobson (1992) and the Appendix). Given the results of the cluster analysis summarized in Tab. 1, we were determined to estimate the axis length distribution of ellipses bounding the clusters. An ellipse centered at the origin with semi-axis lengths $a \geq b > 0$ such that the longer axis is located on the first coordinate axis is denoted by

$$E(a, b, 0) = \{(x_1, x_2)^\top \in \mathbb{R}^2 : \frac{x_1^2}{a^2} + \frac{x_2^2}{b^2} \leq 1\}.$$

image	subject	area (μm^2)	# points	intensity (μm^{-2})	# clusters	# background points	# ellipses
1	1	628 × 469	167	$5.67{\cdot}10^{-4}$	68	51	26
2	2	628 × 469	164	$5.57{\cdot}10^{-4}$	67	54	29
3	2	628 × 469	172	$5.84{\cdot}10^{-4}$	65	59	25
4	3	896 × 671	242	$4.03{\cdot}10^{-4}$	84	62	37
5	3	896 × 671	340	$5.66{\cdot}10^{-4}$	110	89	48
6	3	896 × 671	283	$4.71{\cdot}10^{-4}$	99	95	37
7	4	896 × 671	143	$2.38{\cdot}10^{-4}$	78	88	13
8	4	896 × 671	192	$3.19{\cdot}10^{-4}$	83	80	23

Table 1: Results of the hierarchical cluster analysis for the image data to be modeled. Ellipses were constructed for clusters containing at least 3 points, the remaining cell nuclei were classified as background points.

For $\theta \in [-\pi/2, \pi/2)$ we denote by $E(a, b, \theta)$ the image of $E(a, b, 0)$ under a rotation around the origin by an angle θ.

If we consider a fixed ellipse $E(a, b, 0)$ with $0 < b \leq a$, the points of a homogeneous Poisson process on $E(a, b, 0)$ are conditionally independent and uniformly distributed on $E(a, b, 0)$ given that their number is known. Thus, the question to recover $E(a, b, 0)$ from the realization of a Poisson process restricted to $E(a, b, 0)$ reduces to the task of estimating a and b based on some random vectors $Y_1, \ldots, Y_{\mathsf{N}}$, where $Y_1, Y_2, \ldots$ are independent and uniformly distributed on $E(a, b, 0)$, and the Poisson distributed random variable N is independent of $Y_1, Y_2, \ldots$. The following proposition summarizes basic properties of such random vectors, which are easily verified by elementary computations.

Proposition 1. *Let Y be a* 2D *random vector which is uniformly distributed on $E(a, b, 0)$, then $\mathbb{E}Y = o$ and the covariance matrix Σ_Y of Y is given by*

$$\Sigma_Y = \begin{pmatrix} \frac{a^2}{4} & 0 \\ 0 & \frac{b^2}{4} \end{pmatrix}.$$

This observation will finally lead to estimators for a and b using principal component analysis (PCA) (for details on PCA see e.g. Jollifee (2002)). The first principal component of a random vector Y with $\mathbb{E}(Y^2) < \infty$ is defined as

$$\eta_1 = \max_{\|\xi\|=1} \mathrm{Var}(\xi^\top Y)$$

and the corresponding direction of maximum variance is denoted by

$$\xi_1 = \arg\max_{\|\xi\|=1} \mathrm{Var}(\xi^\top Y).$$

The second principle component is then given by

$$\eta_2 = \max_{\|\xi\|=1} \mathrm{Var}\big(\xi^\top (Y - \xi_1 \xi_1^\top Y)\big)$$

with a corresponding direction of maximum residual variance

$$\xi_2 = \arg\max_{\|\xi\|=1} \mathrm{Var}\big(\xi^\top (Y - \xi_1 \xi_1^\top Y)\big).$$

Since Y is a 2D random vector, it is easily seen that ξ_2 is one of the two unit vectors orthogonal to ξ_1. Moreover, it is well-known that η_1 and η_2 are the eigenvalues of the covariance matrix Σ_Y, whereas ξ_1 and ξ_2 are corresponding eigenvectors of unit length (Jollifee (2002) pp.5). Thus, Proposition 1 entails the following result.

Corollary 2. *Let $Y \sim U(E(a, b, 0))$ with $a > b$, then*

$$\eta_1 = \frac{a^2}{4}, \qquad \eta_2 = \frac{b^2}{4}, \qquad \xi_1 = (1, 0)^\top, \qquad \textit{and} \qquad \xi_2 = (0, 1)^\top.$$

Now we consider the eigenvalues $\widehat{\eta}_1 \geq \widehat{\eta}_2$ of the sample covariance matrix

$$\widehat{\Sigma}_Y = \frac{1}{\mathsf{N} - 1} \sum_{i=1}^{\mathsf{N}} (Y_i - \overline{Y}_{\mathsf{N}})(Y_i - \overline{Y}_{\mathsf{N}})^\top$$

of $Y_1, \ldots, Y_{\mathsf{N}}$, where $\mathsf{N} \geq 2$. For a and b we obtain the natural estimators

$$\widehat{a} = 2\sqrt{\widehat{\eta}_1} \qquad \text{and} \qquad \widehat{b} = 2\sqrt{\widehat{\eta}_2}\,.$$

This defines a method to estimate the semi-axis lengths a and b from a realization of a Poisson process in the ellipse $E(a, b, 0)$ with parallel orientation to the coordinate axes. In a next step we consider ellipses $E(a, b, \theta) + c$ which are rotated by an angle θ and centered at some point $c \in \mathbb{R}^2$. Let O_θ be the orthogonal matrix describing a rotation by an angle $\theta \in [-\pi/2,\, \pi/2)$ around the origin, i.e., in particular $O_\theta^{-1} = O_\theta^\top$. If we consider shifted and rotated versions $O_\theta Y_1 + c, \ldots, O_\theta Y_{\mathsf{N}} + c$ of the random vectors $Y_1, \ldots, Y_{\mathsf{N}}$, we obtain a Poisson process in the ellipse $E(a, b, \theta) + c$. The covariance matrix $\Sigma_{O_\theta Y + c}$ of the transformed random vector $O_\theta Y + c$ is given by

$$\Sigma_{O_\theta Y + c} = O_\theta \Sigma_Y O_\theta^\top.$$

Thus, $\Sigma_{O_\theta Y + c}$ has the same principal components as Σ_Y. This observation and the fact that the columns of O_θ form an orthonormal basis of eigenvectors of $\Sigma_{O_\theta Y + c}$ lead to the following generalization of Corollary 2.

Corollary 3. *Let $Y \sim U(E(a, b, \theta) + c)$ with $a > b$, then*

$$\eta_1 = \frac{a^2}{4}, \qquad \eta_2 = \frac{b^2}{4}, \qquad \xi_1 = (\cos\theta, -\sin\theta)^\top, \text{ and} \qquad \xi_2 = (\sin\theta, \cos\theta)^\top.$$

As a consequence, given a sequence of conditionally independent random vectors $Y_1, \ldots, Y_{\mathsf{N}}$ with $Y_i \sim U\big(E(a, b, \theta) + c\big)$ and $\mathsf{N} \geq 2$ we obtain the natural estimators

$$\widehat{a} = 2\sqrt{\widehat{\eta}_1}, \qquad \widehat{b} = 2\sqrt{\widehat{\eta}_2}, \quad \text{and} \qquad \widehat{\theta} = \arcsin(-\widehat{\xi}_{1,2}) \tag{1}$$

for a, b, and θ, where $\widehat{\eta}_1$, and $\widehat{\eta}_2$ are the eigenvalues of the sample covariance matrix

$\widehat{\Sigma}_Y$, and $\widehat{\xi}_1 = (\widehat{\xi}_{1,1}, \widehat{\xi}_{1,2})^\top$ is an eigenvector of unit length for $\widehat{\eta}_1$ with $\widehat{\xi}_{1,1} \geq 0$. Moreover, given that $\mathsf{N} > 0$, Proposition 1 yields that $\widehat{c} = \overline{Y}_{\mathsf{N}}$ defines an unbiased estimator for the location vector c. It is verified by elementary computations that if in the above definitions the Poisson distributed random variable N is replaced by a deterministic integer $\nu \geq 0$, the assumptions on $Y_1, \ldots, Y_\nu$ entail the strong consistency of the estimators $\widehat{a}$, $\widehat{b}$, and $\widehat{\theta}$ as $\nu \to \infty$, and one can also show asymptotic unbiasedness by a dominated convergence argument. The estimators are however not unbiased as is clearly seen in Fig. 3 (a), where small numbers of points in particular lead to an underestimation of the minor axis length. Note that for the image data we are modeling, the independence assumption of the points is violated since a hardcore radius leads to mutual repulsion of points. However, the simulation results of Fig. 3 (c) and (d) showing the empirical conditional estimation means and standard deviations in the hardcore setting given that $\mathsf{N} = \nu$ indicate that the hardcore effect of our data does not lead to severe distortions of the estimation results in comparison to the independent setting.

In real CH patterns one also finds string-like clusters, where the number of points on the surrounding ellipse is proportional to the major axis length rather than to the ellipse area (Fig. 2). As will be discussed later, these clusters are modeled by a different type of point process constructed by a two-step procedure. In a first step a point process is realized on the major axis of the ellipse, thus yielding points which are concentrated on a line segment. Subsequently, these colinear points are independently and uniformly shifted within the ellipse in parallel direction to the minor axis. In the following the construction of this process is made precise for the

ellipse $E(a, b, 0)$. In the easiest case, given the total number N of points equals ν, the locations $Y_1, \ldots, Y_\nu$ are independent copies of a random vector $Y_0 = (Y_{01}, Y_{02})$, where the first component Y_{01} is uniformly distributed on $(-a, a)$, i.e.,

$$Y_{01} \sim U(-a, a), \tag{2}$$

and the conditional distribution of Y_{02} given Y_{01} is

$$Y_{02} \mid Y_{01} \sim U\left(-b\sqrt{1 - \frac{Y_{01}^2}{a^2}},\ b\sqrt{1 - \frac{Y_{01}^2}{a^2}}\right). \tag{3}$$

Using the definition of the conditional density and elementary computations one obtains the following result.

Proposition 4. *Let Y be a* 2D *random vector which is distributed as defined by* (2) *and* (3)*. Then $\mathbb{E}Y = o$ and the covariance matrix of Y is given by*

$$\Sigma_Y = \begin{pmatrix} \frac{1}{3}a^2 & 0 \\ 0 & \frac{2}{9}b^2 \end{pmatrix}.$$

Comparing the above result to Proposition 1, it is evident that using the estimators defined by (1) to reconstruct the shape of the ellipse from point patterns formed by independent random vectors of this type, the length of the major ellipse axis is overestimated, whereas the minor axis length is slightly underestimated. This effect is illustrated by the simulation results shown in Fig. 4, where we applied the estimators in (1) in the two cases of a Poisson process (as covered by Proposition 4) and a Matérn hardcore process on the major ellipse axis prior to shifting. The simulation results indicate that in the hardcore setting the bias of the estimators only slightly increases in comparison to the Poisson case. Moreover, the bias is relatively stable in the number of points and the length of the minor axis is not severely underestimated.

3.3. Point process model

In this section we describe our point process model for CH patterns to be fitted to the image data. An overview on the stepwise model construction is given in Fig. 5. Shapes and centers of the CH clusters are modeled by an elliptical Matérn hardcore process in $\mathbb{R}^2$ with points $\{X_n\}_{n\geq 1}$ and associated ellipses $\{E(A_n, B_n, \Theta_n)\}_{n\geq 1}$. The first ingredient for the construction of an elliptical Matérn hardcore process is a homogeneous Poisson point process in $\mathbb{R}^2$ with intensity λ_0, where λ_0 denotes the expected number of points in the unit square. Additionally, we consider a sequence of iid random ellipses centered at the Poisson points with independent uniform orientation distribution. These ellipses are in general overlapping. For each clique of overlapping ellipses one of them is selected at random to survive, whereas the others are deleted. For a formal construction of this thinning procedure we refer to the appendix. It is intuitively clear that large ellipses are more likely to be intersected by others than small ones, which results in a decreased survival probability during thinning. It is however not easily possible to determine the ellipse shape distribution before thinning analytically for a given shape distribution after thinning, and thus to estimate the distribution before thinning from a set of image data to be modeled. We nevertheless needed to identify an appropriate joint distribution function for the axis lengths of the typical ellipse $E(A_0, B_0, \Theta_0)$ *before thinning*, and started with an analysis of the marginal distributions of the semi-axes in the microscopy data. These can be adequately approximated by two gamma distributions and hence it seems natural to model the common distribution of the semi-axis lengths by a two-dimensional analogue. Since by definition $0 \leq B_0 \leq A_0$, the support of an appropriate density

function needs to be restricted to the area below the first bisecting line in the first quadrant. These considerations led us to the density

$$f(a,b) = \kappa_f a^2 b^3 e^{-(pa+qb)} \mathbb{1}_{\{0\le b\le a\}}, \tag{4}$$

for some parameters $p, q > 0$, and a normalizing constant κ_f. Note that κ_f needs not to be explicitly known in order to sample from the density f using a rejection sampler. More precisely, a realization of a random vector with density f is obtained by repeated realization of two independent random variables $Z_a \sim \Gamma(3,p)$ and $Z_b \sim \Gamma(4,q)$ until $Z_a \ge Z_b$.

Given the marked point process $X_M = \{(X_n, E(A_n, B_n, \Theta_n))\}_{n\ge1}$ representing the non-overlapping ellipses, we construct finite child point processes $Y^{(n)} = \{Y_k^{(n)}\}$ on the ellipses $E(A_n, B_n, \Theta_n) + X_n$ and a background point process $Y^{(B)} = \{Y_k^{(B)}\}_{k\ge1}$ outside the ellipses. The child processes $Y^{(n)}$ on the random ellipses are independent and modeled by two different hardcore processes with hardcore distance $r > 0$, where the choice of the model depends on ellipse thickness. In case $B_n > r$, an ellipse is classified as thick and its associated child process is defined as the restriction of an ordinary Matérn hardcore process $Z^{(n)} = \{Z_k^{(n)}\}_{k\ge1}$ on $\mathbb{R}^2$ with hardcore radius r and intensity $\lambda_1 > 0$ to the ellipse $E(A_n, B_n, \Theta_n) + X_n$, i.e.,

$$Y^{(n)} = Z^{(n)} \cap (E(A_n, B_n, \Theta_n) + X_n).$$

An ordinary Matérn hardcore process is defined as the more general elliptical model introduced above with all ellipses given by the deterministic disc $B(\boldsymbol{o}, \frac{r}{2})$.

In view of our data, the number of points in thin ellipses (satisfying $B_n \le r$) depends

primarily on the length of the major axis and not on the area of the ellipse. Clusters on thin ellipses are therefore modeled by 1D Matérn hardcore processes on the major ellipse axis, whose points are then independently and uniformly shifted within the ellipse in parallel direction to the minor axis. For a formal definition we consider a fixed thin ellipse $E(a, b, 0)$ in parallel orientation to the coordinate system and a Matérn hardcore process $\{Z_{1k}^{(n)}\}_{k\geq 1}$ on $\mathbb{R}^1$ with hardcore radius r and intensity $\lambda_2 > 0$. The child process on $E(a, b, 0)$ is then defined as

$$Y^{(n)} = \{(Z_{1k}^{(n)}, Z_{2k}^{(n)})\}_{k\geq 1} \cap E(a, b, 0),$$

where the distribution of $Z_{2k}^{(n)}$ conditioned on $Z_{1k}^{(n)} \sim U(-a, a)$ was defined in (3). For an ellipse $E(a, b, \theta) + x$ in general position we consider an appropriately rotated and shifted version of the above process.

Since for the analysis of our microscopy data, ellipses could only be estimated for clusters of at least 3 points, ellipses containing less than 3 points are discarded in the model and our point process representing CH patterns is finally defined as

$$Y = Y^{(B)} \cup \bigcup_{n:\, |Y^{(n)}|\geq 3} Y^{(n)},$$

where $|Y^{(n)}|$ denotes the number of points of $Y^{(n)}$.

It remains to specify the process $Y^{(B)}$ of background points. For this we consider the random subset W_{X_M} of $\mathbb{R}^2$ which is not covered by the (slightly enlarged) ellipses, i.e.,

$$W_{X_M} = \mathbb{R}^2 \setminus \bigcup_{n:\, |Y^{(n)}|\geq 3} \big(E(A_n, B_n, \Theta_n) + X_n\big) \oplus B(\boldsymbol{o}, \rho), \tag{5}$$

where $\oplus$ denotes the dilation $A \oplus B = \{x + y : x \in A, y \in B\}$ of two sets $A, B \subset \mathbb{R}^2$. The background point process is then defined as $Y^{(B)} = \widetilde{Y}^{(B)} \cap W_{X_M}$, where $\widetilde{Y}^{(B)}$ is an ordinary Matérn hardcore process with fixed hardcore radius r and intensity $\lambda_3 > 0$ on $\mathbb{R}^2$. The parameter ρ specifies the repulsion effects of the ellipses on the background points. The dilation of the ellipses by the disc $B(\boldsymbol{o}, \rho)$ in (5) ensures that the background points keep a minimal distance ρ from the ellipses.

3.4. Model fitting

In order to fit the point process model described in the preceding section to our CH data we need to estimate the following parameters:

- The hardcore radius r,
- the repulsion parameter ρ
- the intensity λ_0 of the Poisson process used to define the elliptical Matérn hardcore process governing cluster shapes and locations,
- the intensity λ_1 of the Matérn hardcore process on the thick ellipses,
- the linear intensity λ_2 controlling the child process on the thin ellipses,
- the intensity λ_3 of the background point process, and finally
- the parameters p, q for the density f (see (4)) controlling the axis distribution of the ellipses before thinning.

The process of model fitting explained below is summarized in Fig. 6. For our CH data, the hardcore radius r and the repulsion parameter ρ were not estimated from

the data but set to the values $r = 7.5\mu m$ and $\rho = 3.5r$, respectively. These were natural choices in view of the minimum inter-point-distances after data preprocessing and the stopping criterion during cluster analysis (see Section 2 and the Appendix). However, for general applications of the model, the hardcore radius r may be directly estimated from the data as $\widehat{r} = \min_{\substack{i \neq j \\ k=1,\ldots,K}} \|y_{ki} - y_{kj}\|$, where $\{y_{k1}, \ldots, y_{k\nu_k}\}$ are the nucleus coordinates of image k. Moreover, the repulsion parameter ρ may be estimated as the minimal distance of the background points to the ellipses.

The extracted ellipses were classified as thick or thin, depending on whether their minor semi-axis exceeded $r = 7.5\mu m$ or not.

In order to specify estimators for the remaining parameters we introduce the following notation. For the kth image, where $k = 1, \ldots, K$, and ellipses constructed as described above we denote by

- W_k the observation window corresponding to the kth image,
- $N_1^{(k)}$ the number of the points in thick ellipses in W_k,
- $N_2^{(k)}$ the number of the points in thin ellipses in W_k,
- $N_3^{(k)}$ the number of background points in W_k,
- $\hat{E}_1^{(k1)}, \ldots, \hat{E}_{n_1(k)}^{(k1)}$ the estimated thick ellipses in W_k,
- $\left(\hat{a}_1^{(k1)}, \hat{b}_1^{(k1)}\right), \ldots, \left(\hat{a}_{n_1(k)}^{(k1)}, \hat{b}_{n_1(k)}^{(k1)}\right)$ the estimated lengths of the corresponding semi-axes,
- $\hat{E}_1^{(k2)}, \ldots, \hat{E}_{n_2(k)}^{(k2)}$ the estimated thin ellipses in W_k,

- $\left(\hat{a}_1^{(k2)}, \hat{b}_1^{(k2)}\right), \ldots, \left(\hat{a}_{n_2(k)}^{(k2)}, \hat{b}_{n_2(k)}^{(k2)}\right)$ the estimated lengths of the corresponding semi-axes, and

- $\hat{\ell}_1^{(k)}, \ldots, \hat{\ell}_{n_2(k)}^{(k)}$ the intersection lengths of the major axes in the thin ellipses with W_k.

This leads to the following natural estimators for λ_1, λ_2, and λ_3. We define

$$\hat{\lambda}_1 = \frac{\sum_{k=1}^K N_1^{(k)}}{\sum_{k=1}^K |\bigcup_{i=1}^{n_1(k)} E_i^{(k1)} \cap W_k|}, \qquad \hat{\lambda}_2 = \frac{\sum_{k=1}^K N_2^{(k)}}{\sum_{k=1}^K \sum_{i=1}^{n_2(k)} \hat{\ell}_i^{(k)}}, \qquad \text{and}$$
$$\hat{\lambda}_3 = \frac{\sum_{k=1}^K N_3^{(k)}}{\sum_{k=1}^K |W_k \setminus (\bigcup_{j=1}^2 \bigcup_{i=1}^{n_j(k)} (\hat{E}_i^{(kj)} \oplus B(\boldsymbol{o}, \rho))|}.$$

As will be demonstrated below and illustrated in Fig. 7, the joint axis length distribution of the typical ellipse in the image data was well reproduced by the model when the axis length distribution before thinning was given by the density f defined in (4) which was fitted to the joint axis distribution computed from the image data. This way we neglected the difference between the distribution of a typical ellipse before and after thinning in the elliptical Matérn hardcore process, which has been discussed in Section 5.2. The simulation results in Fig. 7 indicate that the resulting increase in the likelihood of small ellipses was however compensated for, when, after completion of the thinning process, ellipses with less than three points were discarded. In summary, Fig. 7 suggests that the final simulated joint axis length distribution of the retained ellipses after thinning and discarding of ellipses containing less than three child points was in satisfactory agreement with the axis length distribution of the ellipses extracted from the image data.

The parameters p and q for the density f of (A_0, B_0) given in (4) were fitted by

parameter	value	mean	standard deviation	p-value
p	$7.7 \cdot 10^{-2}$	$7.98 \cdot 10^{-2}$	$2.77 \cdot 10^{-3}$	0.398
q	0.496	0.456	0.03	0.166
λ_0	$1.25 \cdot 10^{-4}$	$1.07 \cdot 10^{-4}$	$1.43 \cdot 10^{-5}$	0.202
λ_1	$3.07 \cdot 10^{-3}$	$3.04 \cdot 10^{-3}$	$1.83 \cdot 10^{-4}$	0.878
λ_2	$5.24 \cdot 10^{-2}$	$5.37 \cdot 10^{-2}$	$1.11 \cdot 10^{-3}$	0.318
λ_3	$2.47 \cdot 10^{-4}$	$2.77 \cdot 10^{-4}$	$9.77 \cdot 10^{-6}$	0.004

Table 2: Empirical estimation means and standard deviations when model parameters were repeatedly fitted to samples of 8 realizations of the point process model. The true model parameters given in the first column represent the estimation results for the microscopy data. p-values refer to Monte-Carlo tests investigating the hypothesis that the true parameters are drawn from the distribution underlying the samples of estimation results.

numerical minimization of the loss function

$$L_1(p,q) = \left\| \left(\bar{a}, \bar{b}\right) - \mathbb{E}_{p,q}\left(A_0, B_0\right) \right\|,$$

where $\bar{a}$ and $\bar{b}$ denote the mean estimated lengths of the major and minor semi-axes in the data. Thus, we used the moment estimator $(\widehat{p}, \widehat{q}) = \arg\min L_1(p,q)$ for (p,q). It remained to estimate the parameter λ_0 determining the intensity of the ellipse centers before thinning in the elliptical Matérn hardcore process. For this purpose we used an estimator obtained by numerical minimization of the loss function

$$L_2(\lambda_0) = |\hat{\lambda} - \lambda(\lambda_0)|,$$

measuring the difference between the total empirical intensity

$$\widehat{\lambda} = \frac{\sum_{k=1}^{K}(N_1^{(k)} + N_2^{(k)} + N_3^{(k)})}{\sum_{k=1}^{K}|W_k|}$$

in the data and a Monte-Carlo estimate of the model intensity $\lambda(\lambda_0)$. We finally set $\widehat{\lambda}_0 = \arg\min L_2(\lambda_0)$.

3.5. Stability of the fitting method

The stability of the fitting methodology introduced in the preceding sections was scrutinized by a refitting procedure. For this purpose we simulated 8 realizations of the point process model with the parameters that were estimated when analyzing the microscopy data. For these 8 simulated datasets, the fitting procedure including the cluster analysis was conducted resulting in a set of estimated model parameters. This procedure of point process model realization and successive estimation of associated model parameters was performed 999 times yielding 999 estimation results, which were then compared to the real model parameters underlying the simulated point patterns. This way the stability of our statistical fitting method was assessed. The average estimation results were in close proximity to the actual model parameters despite the theoretical bias of some estimators. In addition, they exhibited only small standard deviations, which were a magnitude smaller than the corresponding means (Tab. 2). Based on the samples of estimated model parameters we conducted Monte-Carlo tests inferring whether the actual model parameters can be regarded as sampled from the distribution of the estimation results. The p-values in Tab. 2 indicate that all but one model parameter were not significantly different from the estimated counterparts, thus demonstrating the stability of our fitting method. Note that we did not correct for multiple testing, since this would have been in favor of our method. In summary, the fitting methodology (including the cluster analysis) recovers the model parameters rather adequately in the given setting of parameters and for observation windows of size and number similar to the microscopy data. The only parameter that deviated significantly from the estimation results is the intensity

of the background points ($p = 0.004$), which on average exceeds the actual value by $\sim 12\%$. This may be related to the observation that in the model some child point processes within the ellipses include points with nearest neighbors farther away than $\rho = 22.5\mu m$, which is the stopping distance for the cluster analysis. These points are hence classified as background points by the cluster analysis instead of being associated with an ellipse.

3.6. Model validation

In order to validate the model we compared several image characteristics of simulated and microscopy data on a descriptive level. More precisely, we investigated the pair-correlation function, the nearest neighbor distance and the spherical contact distributions, which were selected on the presumable biologic relevance of the morphological image properties they capture. The pair-correlation function $g : [0, \infty) \longrightarrow [0, \infty)$ of the point patterns monitors clustering and repulsion effects of the points. For a mathematical definition of g we refer to Illian et al. (2008). Heuristically interpreted, $g(r) < 1$ implies that point pairs of distance r are less likely to occur in the analyzed point patterns than in a Poisson point process of equal intensity, which indicates repulsion of points at this distance. On the other hand, clustering of points is indicated if $g(r) > 1$ for some value $r > 0$, which means that there are statistically more point pairs of distance r than in a Poisson process. Since clustering of CHs is found in healthy cartilage, whereas the organization of the cells in clusters breaks down in osteoarthritic cartilage (Rolauffs et al. (2011)), the pair-correlation function assesses a biologically relevant morphological characteristic which should be reproduced by a suitable point process model. Fig. 8 (a) shows

an empirical 90% confidence band which was obtained by sampling from our model and a distance-wise computation of empirical quantiles. One sees that the hardcore effect of the data and the peaks of the pair-correlation functions from the three sets of microscopy data are captured rather well. Thus, hardcore and clustering effects are similar in the model and the image data. Moreover, the variability of the model seems to be comparable to the real data, even if the variations of peak height for the 8 analyzed microscopy images was slightly larger than observed in the model. The second characteristic we considered for model validation is the nearest-neighbor-distance distribution function (NNDDF) $D : [0, \infty) \longrightarrow [0, 1]$. For a stationary point processes $Y = \{Y_n\}_{n\geq 1}$ (without multiple points) and intensity $\lambda > 0$ observed on an arbitrary window W of positive volume, $D(r)$ is defined as

$$D(r) = \frac{1}{\lambda |W|} \mathbb{E} \sum_{n\geq 1} \mathbb{1}_{\{Y_n \in W,\, \min_{m\neq n} \|Y_m - Y_n\| \leq r\}}.$$

From a biological point of view, the distance of the CHs to their nearest neighbor is important for the effectiveness of fluid-flow-related or diffusion-driven chemical signal transduction between cells. Fig. 8 (b) shows pointwise empirical confidence intervals of the estimated model NNDDF and corresponding estimation results for the cartilage image data. For r between 18 and $30\mu m$ the mean NNDDF of the microscopy data is slightly larger than the upper envelope of the model NNDDF, which nevertheless captures some of the images (corresponding to subject 4) rather well.

As a third characteristic for model validation we estimated the spherical contact distribution function (SCDF) $H : [0, \infty) \longrightarrow [0, 1]$ of the point patterns, which for a

stationary point process $Y = \{Y_n\}_{n\geq 1}$ is defined as

$$H(r) = P(\min_{n\geq 1} \|Y_n\| \leq r).$$

For our cartilage data, the SCDF assesses the distance distribution of an arbitrarily chosen location on the cartilage surface to the next CH nucleus. This distribution contains information which is biologically relevant for the transport of cytokines and newly synthesized molecules to an arbitrarily chosen articular surface point. As can be seen in Fig. 8 (c), the mean SCDF estimated from the data is in highly satisfactory agreement with the model. Nevertheless, the SCDFs of subjects 1 and 4 show rather large deviations from the mean of the microscopy data, which are beyond the variability of the model. Taking into account the pair-correlation function of subject 1, the CH pattern in this sample seems to be relatively regular in comparison to the other images, which explains increased values of the SCDF. Subject 4 on the other hand exhibited a substantially decreased intensity of the CH patterns, which naturally decreases the SCDF.

For the estimation of the three characteristics we used standard estimators, which can e.g. be found in Illian et al. (2008). Notice that all three functions considered for model validation have not been used for model fitting and thus represent extrinsic measures for the goodness of model fit.

Apart from the three characteristics discussed above, the fractions of points falling into thick and thin ellipses and the fraction of background points are very similar in the image data and the model simulations (Tab. 3). This should however already be ensured by the model fitting algorithm. We finally remark that the fraction of

	real image data	model simulations
Points on thick ellipses	34%	32%
Points on thin ellipses	32%	35%
Background points	34%	33%

Table 3: Fractions of different points types in the real image data and the simulations.

ellipses classified as thin was 56% in the cartilage images and 54% in the simulations, which is another indicator that the presented model is able to adequately describe and simulate a mean scenario of the observed organizational structure in superficial CH patterns *in silico*.

4. Discussion

In this study we investigated whether the spatial organization of superficial CH can be characterized by a point process model. Presenting a suitable point process model that describes the CH patterns within the articular surface of intact human knee cartilage, we conclude that these can adequately be modeled by a stochastic point process consisting of non-overlapping elliptical point clusters. We demonstrated that this type of model is well-suited to realistically represent the mean biological scenario of the occurring cellular patterns. Moreover, we were able to represent the complex morphology of the organizational structure of articular CHs by a set of 8 model parameters, which implies a substantial reduction of complexity in comparison to the original image data. This approach opens new perspectives for a model-based statistical analysis and classification of CH patterns in both intact and osteoarthritic tissues. The latter is particularly important because degeneration of cartilage due to OA has been demonstrated to coincide with spatial changes in the superficial CH organization (Rolauffs et al. (2011)). Further elucidation of such pattern-associated

pathology may broaden our understanding of the early events during OA onset and may hopefully lead to the development of quantitative decision support systems in diagnosis, which will be a subject of our future research. The link between the geometric structure of CH patterns and functional properties of cartilage strongly suggests using tools from statistical image analysis for quantitative decision support systems in diagnostics of OA. This requires an interdisciplinary approach combining capabilities in imaging, biology, and spatial statistics. Since promising novel imaging techniques for the visualization of cartilage surface will likely be available in the near future (Schenke-Layland (2008)), we started the development of an appropriate statistical methodology by constructing a stochastic model for the morphology of CH patterns in intact cartilage. This model may serve as a reference for a future statistical analysis investigating deviations of cartilage image data from the healthy state. The task to develop realistic models for point patterns frequently leads to situations where compromises between analytical tractability of the model and the quality of data representation need to be made. In the present study our primary interest was to adequately represent the observed data since such emphasis is naturally crucial for future model-based automated diagnostic tools. The analytical tractability of point processes is mostly tied to the presence of Poisson components in the model. Although generalized Matern hardcore processes, as used in our study, are constructed by thinning of Poisson point processes, their analytical tractability is typically limited once the geometry of the random hardcore areas around points becomes moderately complex (see also Månsson and Rudemo (2002)). This applies in particular to elliptical hardcore processes. Consequently, even for basic model

characteristics explicit formulas seem hard to be obtained. On the other hand, this type of model can be used to generate the wide range of shape variability of CH clusters necessary to represent the biological variability occurring in different joint surfaces and states of disease. In the present study we fitted the model to data from the intact cartilage of the human knee joint condyles since the images of these areas represent a rather complex morphological scenario of human cartilage exhibiting a co-existence of strings, clusters, pairs, and single CHs (Rolauffs et al. (2008)). However, we paid attention to ensure a certain versatility of our model to abet our future efforts to model CH patterns in different types and states of cartilage other than the scenario considered here. Preliminary experiments with data recorded from patients with OA indicated that osteoarthritic cartilage can also be adequately described by our point process model. This will be the subject of a forthcoming paper. One of the main goals of the present study was to develop an appropriate fitting methodology for the point process model. In experiments with established minimum contrast methods for the fitting of point processes using Ripleys K-function or the pair-correlation function (Heinrich (1992); Illian et al. (2008); Stoyan (1992)) we observed that these approaches failed to satisfactorily reproduce cluster shapes. We therefore established a method for the estimation of the cluster shape distribution directly from the image data. For this purpose we combined a hierarchical cluster analysis with an approach inspired by PCA to extract clusters and corresponding surrounding ellipses from the images. This allowed to estimate the shape distribution of ellipses surrounding CH clusters of at least 3 cells. Single and paired CHs were taken into account by fitting an appropriate background point process. As pointed out,

some theoretical properties such as the bias of certain estimators are not necessarily ideal. However, as demonstrated, we obtained a good fit of our model. Moreover, our refitting experiments indicate the stability of the statistical fitting methodology for data exhibiting the structure and sample size used in our study. Our results for model validation indicate that the point process accurately captures important mean geometric characteristics of the observed data such as nearest neighbor distance and the spherical contact distribution. The variability of the microscopy data suggests that future applications of the model may in particular require fitting of the model to sample images of homogeneous intensity in the CH patterns, since intensity variations naturally entail alterations of other structural characteristics such as the spherical contact distribution. We chose three characteristics for model validation: the nearest-neighbor distance distribution function (NNDDF), the spherical contact distribution function (SCDF), and the pair-correlation function. These functions were used for model validation, because we previously determined that changes in the nearest-neighbor distance as well as in the type and density of the occurring patterns were strongly associated with distinct stages of OA (Rolauffs et al. (2011)). Thus, the 3 functions assess characteristics of presumably high biological relevance. We would like to point out the novelty of this approach since, to the best of our knowledge, none of the functions has been applied previously to study the cellular organization of cartilage. However, since they examine specific characteristics of cellular clusters, they seem appropriate for this task. The shapes of cellular clusters are thought to derive from cellular proliferation and migration, and the formation and specific organization of the ECM during joint development and maturation (Youn

et al. (2006); Morrison et al. (1996); Chi et al. (2004)). The functional roles of CH groups in cartilage functioning, maintenance and degeneration are not well understood. In intact cartilage, CH grouping is functionally relevant because the CHs usually share a common pericellular matrix (PCM) capsule (Hunziker (1992); Poole (1992)) involved in maintaining the extracellular matrix necessary for resistance, absorption, and redistribution of the occurring biomechanical forces during daily life. In OA, the term cluster is widely used to describe the increased numbers and sizes of cell groups that are an OA hallmark feature detectable near fissures and clefts of the articular surface in the majority of specimens (Lotz et al. (2010))). Importantly, the clearly defined organizational patterns of intact cartilage are lost in osteoarthritic cellular clustering, in which an unordered proliferation resulting in hypercellular areas is a feature of early OA onset (Rolauffs et al. (2011)). This cell proliferation is presumably driven by a variety of growth factors expressed in the clusters (Lotz et al. (2010)) resulting in differences in shape, location, number, and biosynthetic activity of cells within particular groups suggesting that two types of groups with different functions are present in the two tissues. Further joint studies planned in our research groups will attempt to link biologically relevant characteristics utilizing the presented model. We strongly believe that, if these attempts will succeed, a need for statistical classification tools of cartilage image data will arise. Point process models providing realistic descriptions of articular CH patterns may become key ingredients in future model-based statistical analyses of microscopy data and the development of quantitative diagnostic tools.

5. Appendix

5.1. Cluster analysis

Clusters of CH nuclei in the microscopy data were identified by hierarchical cluster analysis using the single linkage method (see e.g. Arabie et al. (1996); Jobson (1992)). In the initial step of this algorithm each point is considered as a single cluster. Then an iterative procedure is started, which merges clusters of minimum distance to enlarge the clusters, where for the single linkage method the distance of two clusters is defined as the minimum distance of two points taken from the two sets. In principle the merging procedure is continued until all points form a single cluster. Nevertheless, in order to obtain a meaningful result, the process is stopped when the distance of the clusters to be merged in the next step exceeds a certain threshold ρ. In our dataset we defined $\rho = 3.5r$, where r denotes the hardcore radius. The cluster analysis identified between 65 and 110 clusters with at least 3 points per image. Slight variations of ρ did not substantially alter the result. Bounding ellipses were constructed for clusters containing at least 3 points (Fig. 2). In principle, the method also identifies single and paired CHs .

5.2. Elliptical Matérn hardcore processes

In the following we introduce the construction principle of elliptical Matérn hardcore processes, which are a special case of so-called *generalized Matérn hardcore processes* as studied in Månsson and Rudemo (2002). We consider a sequence $\{(A_n, B_n)\}_{n\geq 1}$ of independent and identically distributed (iid) random vectors on $[0,\infty)^2$ satisfying $B_n \leq A_n$ and $\mathbb{E}A_n^2 < \infty$. Moreover, $\{\Theta_n\}_{n\geq 1}$ denotes an iid sequence of random angles which is independent of $\{(A_n, B_n)\}_{n\geq 1}$, where we assume

that $\Theta_n \sim U[-\pi/2, \pi/2)$, i.e., Θ_n has a uniform distribution on $[-\pi/2, \pi/2)$. This defines a sequence of random ellipses $\{\Xi_n\}_{n\geq 1}$, where

$$\Xi_n = E(A_n, B_n, \Theta_n).$$

In order to define an elliptical Matérn hardcore process, we consider the random set,

$$\Xi = \bigcup_{n\geq 1} (\Xi_n + X_n), \tag{6}$$

where the random locations $\{X_n\}_{n\geq 1}$ are given by a stationary Poisson process $X = \{X_n\}_{n\geq 1}$ in $\mathbb{R}^2$ with intensity λ_0. The system of ellipses in (6) may contain overlaps. In order to construct a system of points surrounded by non-overlapping ellipses, we apply a random thinning procedure deciding which of the overlapping ellipses are retained and which are removed. The technical details are as follows. If we introduce a sequence of independent random variables $\{U_n\}_{n\geq 1}$, which are uniformly distributed on the interval $(0, 1)$ and independent of X and $\{\Xi_n\}_{n\geq 1}$, the *elliptical Matérn hardcore process* $\widetilde{X}$ is defined as

$$\widetilde{X} = \left\{ X_n : \; U_n = \min\{U_i : \; (\Xi_i + X_i) \cap (\Xi_n + X_n) \neq \emptyset\} \right\}.$$

Thus, a Poisson point X_n marked by U_n is only retained if the shifted ellipse $\Xi_n + X_n$ is not intersected by another shifted ellipse $\Xi_i + X_i$ with a smaller mark $U_i < U_n$. The retaining probability of an ellipse is clearly shape and size dependent. Therefore, the joint distribution of the typical axis length pair $(\widetilde{A}_0, \widetilde{B}_0)$ of the ellipses after thinning differs from the distribution of the typical axis length pair (A_0, B_0) before thinning.

Arabie, P., Hubert, L., De Soete, G., 1996. Clustering and Classification. World Scientific, Singapore.

Chi, S., Rattner, J., Matyas, J., 2004. Communication between paired chondrocytes in the superficial zone of articular cartilage. J. Anat. 205 (5), 363–370.

Choi, J., Youn, I., Cao, L., Leddy, H., Gilchrist, C., Setton, L., Guilak, F., 2007. Zonal changes in the three-dimensional morphology of the chondron under compression: the relationship among cellular, pericellular, and extracellular deformation in articular cartilage. J. Biomech. 40 (12), 2596–2603.

Heinrich, L., 1992. Minimum contrast estimators for parameters of spatial ergodic point processes. In: Transactions 11^{th} Prague Conference on Random Processes, Information Theory and Statistical Decision Functions. Academia, Prague, pp. 479–492.

Hunziker, E., 1992. Articular cartilage structure in humans and experimental animals. In: Kuettner, K., Schleyerbach, R., Peyron, J., Hascall, V. (Eds.), Articular Cartilage and Osteoarthritis. Raven Press, New York, pp. 183–199.

Illian, J., Penttinen, H., Stoyan, H., Stoyan, D., 2008. Statistical Analysis and Modelling of Spatial Point Patterns. J. Wiley & Sons, Chichester.

Jadin, K., Wong, B., Bae, W., Li, K., Williamson, A., et al., 2005. Depth-varying density and organization of chondrocytes in immature and mature bovine articular cartilage assessed by 3d imaging and analysis. J. Histochem. Cytochem. 53 (9), 1109–1119.

Jobson, J., 1992. Applied Multivariate Data Analysis, Volume II: Categorical and Multivariate Methods. Springer, New York.

Jollifee, I., 2002. Principal Component Analysis, 2nd Edition. Springer, New York.

Kuettner, K., Aydelotte, M., Thonar, E., 1991. Articular cartilage matrix and structure: a minireview. J. Rheumatol. Suppl. 27, 46–48.

Lotz, M., Otsuki, S., Grogan, S., Sah, R., Terkeltaub, R., et al., 2010. Cartilage cell clusters. Arthritis Rheum. 62 (8), 2206–2218.

Månsson, M., Rudemo, M., 2002. Random patterns of nonoverlapping convex grains. Adv. Appl. Prob. 34 (4), 718–738.

Morrison, E., Ferguson, M., Bayliss, M., Archer, C., 1996. The development of articular cartilage: I. the spatial and temporal patterns of collagen types. J. Anat. 189 (Pt 1), 9–22.

Muehleman, C., Bareither, D., Huch, K., Cole, A., Kuettner, K., 1997. Prevalence of degenerative morphological changes in the joints of the lower extremity. Osteoarthr Cartilage 5 (1), 23–37.

Poole, C., 1992. Chondrons: the chondrocyte and its pericellular microenvironment. In: Kuettner, K., Schleyerbach, R., Peyron, J., Hascall, V. (Eds.), Articular Cartilage and Osteoarthritis. Raven Press, New York, pp. 201–220.

Poole, C., 1997. Articular cartilage chondrons: form, function and failure. J. Anat. 191 (1), 1–13.

Rolauffs, B., Rothdiener, M., Bahrs, C., Badke, A., Weise, K., et al., 2011. Onset of pre-clinical osteoarthritis: The angular spatial organization permits early diagnosis. Arthritis Rheum. (to appear).

Rolauffs, B., Williams, J., Aurich, M., Grodzinsky, A., Kuettner, K., et al., 2010. Proliferative remodeling of the spatial organization of human superficial chondrocytes distant from focal early osteoarthritis. Arthritis Rheum. 62 (2), 489–498.

Rolauffs, B., Williams, J., Grodzinsky, A., Kuettner, K., Cole, A., 2008. Distinct horizontal patterns in the spatial organization of superficial zone chondrocytes of human joints. J. Struct. Biol. 162 (2), 335–344.

Schenke-Layland, K., 2008. Non-invasive multiphoton imaging of extracellular matrix structures. J. Biophotonics 1 (6), 451–462.

Schumacher, B., Su, J., Lindley, K., Kuettner, K., Cole, A., 2002. Horizontally oriented clusters of multiple chondrons in the superficial zone of ankle, but not knee articular cartilage. Anat. Rec. 266 (4), 241–248.

Stockwell, R., Meachim, G., 1979. The chondrocytes. In: Freeman, M. (Ed.), Adult Articular Cartilage, 2nd Edition. Pitman Medical, Tunbridge Wells, pp. 69–144.

Stoyan, D., 1992. Statistical estimation of model parameters of planar Neyman-Scott cluster processes. Metrika 39 (1), 67–74.

Youn, I., Choi, J., Cao, L., Setton, L., Guilak, F., 2006. Zonal variations in the three-dimensional morphology of the chondron measured in situ using confocal microscopy. Osteoarthr. Cartilage 14 (9), 889–897.

6. Figures

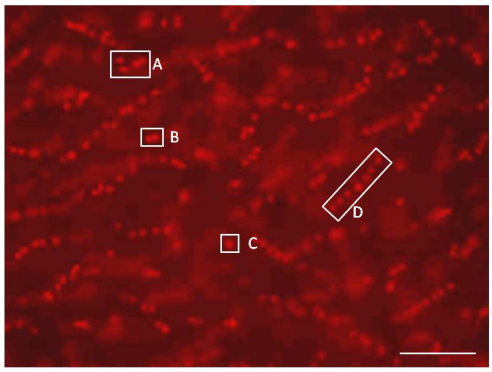

Figure 1: Chondrocyte patterns in the superficial zone of the condyle of the human knee joint. Representative fluorescence microscopy image showing cell nuclei stained with propidium iodide. A: example of a small 4-cell chondrocyte cluster, B: chondrocyte pair, C: single chondrocyte, D: string of chondrocytes based on (Rolauffs et al. (2008)). Fig. 2 (top left) shows the corresponding coordinate plot. Scale bar, 100 μm.

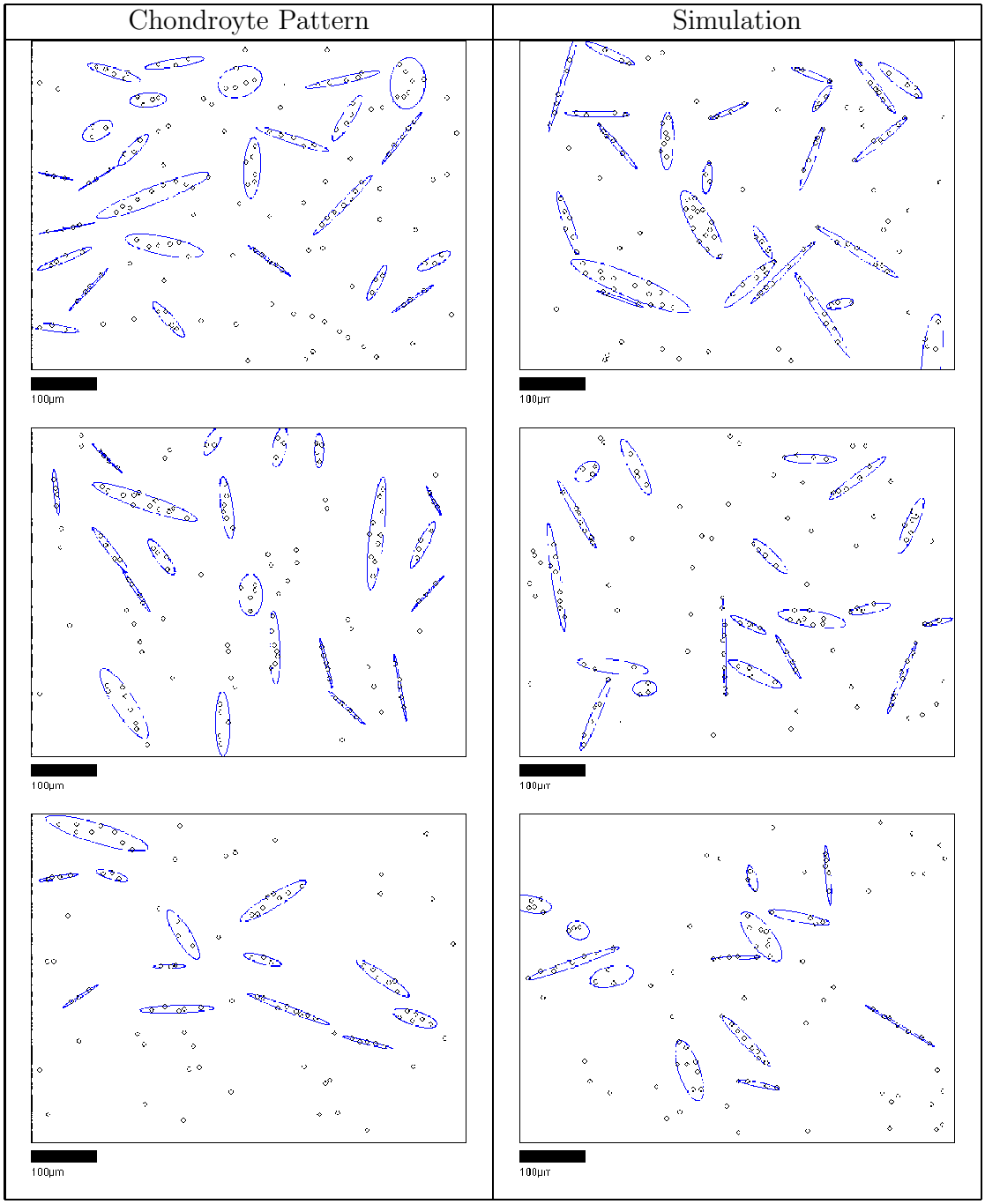

Figure 2: Chondrocyte patterns on the surface of human cartilage from the knee observed by microscopy (left) in comparison to model realizations (right). Rows correspond to a high, medium, and small intensity of the point patterns. The ellipses in the images showing microscopy data (left) were constructed from point clusters identified by hierarchical cluster analysis with at least 3 points, those in the model realizations (right) are defined by the underlying elliptical Matérn hardcore process. Note that the point process model whose realizations are shown on the right has been fitted to a total of 8 images including the three data sets on the left. The remaining images are provided as supplementary material.

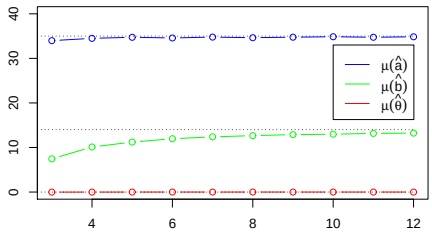

(a) Poisson process

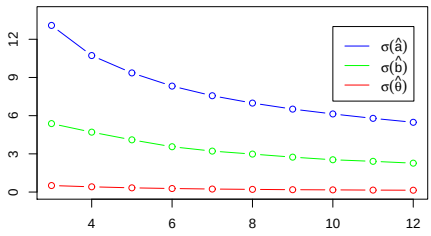

(b) Poisson process

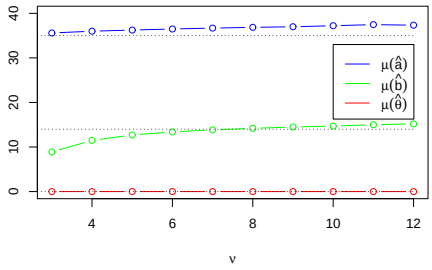

(c) Hardcore process

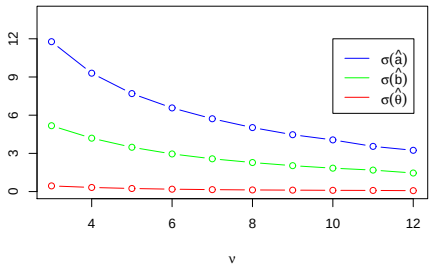

(d) Hardcore process

Figure 3: Empirical conditional means $\mu(\hat{a})$, $\mu(\hat{b})$, $\mu(\hat{\theta})$ and standard deviations $\sigma(\hat{a})$, $\sigma(\hat{b})$, $\sigma(\hat{\theta})$ for the estimators of the parameters a, b, and θ of the fixed ellipse $E_0 = E(35, 14, 0)$ given that the total number of points in E_0 equals ν. Note that the ellipse E_0 is rather average for the thick ellipses in our data. The results in (a) and (b) were obtained for a Poisson process in the ellipse, whereas in (c) and (d) we simulated a Matérn hardcore process with hardcore radius as estimated from the chondrocyte patterns.

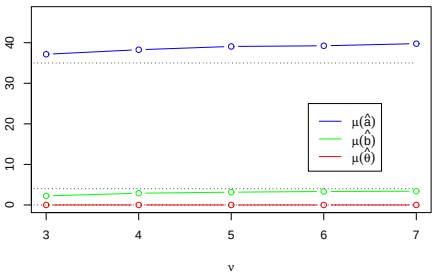

(a) Poisson process

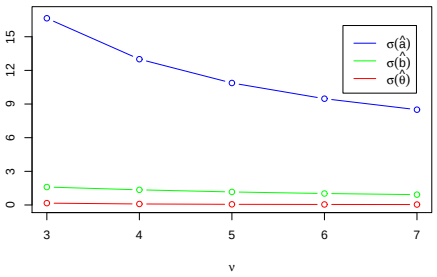

(b) Poisson process

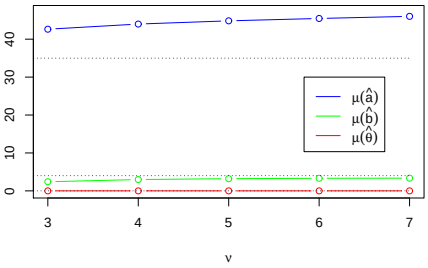

(c) Hardcore process

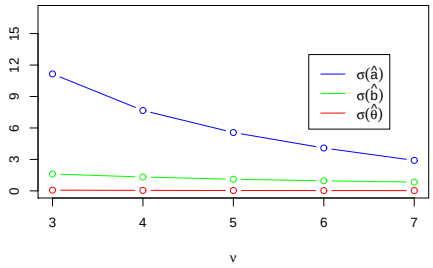

(d) Hardcore process

Figure 4: Empirical conditional means $\mu(\hat{a})$, $\mu(\hat{b})$, $\mu(\hat{\theta})$ and standard deviations $\sigma(\hat{a})$, $\sigma(\hat{b})$, $\sigma(\hat{\theta})$ for the estimators of the parameters a, b, and θ of the fixed ellipse $E_0 = E(35, 4, 0)$ given that the total number of points in E_0 equals ν. Note that the ellipse E_0 is rather average for the thin ellipses in our data. The point patterns were obtained by realizations of linear point processes on the major ellipse axis whose points were then independently and uniformly shifted within the ellipse in perpendicular direction to the major axis. In (a) and (b) prior to shifting, locations were given by Poisson processes on the major axis, whereas in (c) and (d) we simulated Matérn hardcore processes with hardcore radius as estimated from the chondrocyte patterns. We applied the parameter estimators given in (1), which are constructed for ordinary 2D Poisson processes on an ellipse, which leads to a bias for the point processes considered here.

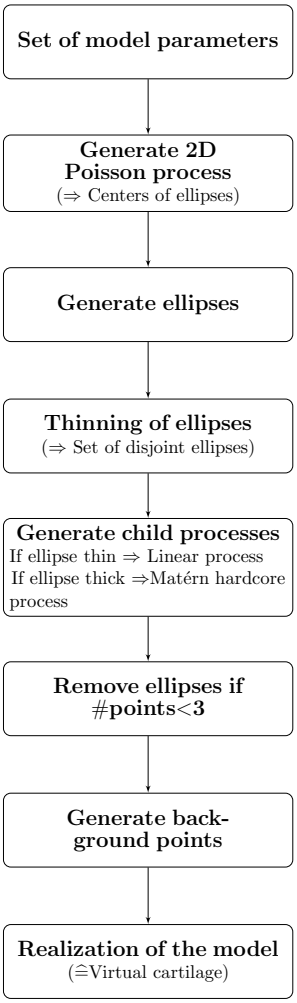

Figure 5: Simulation of chondrocyte patterns.

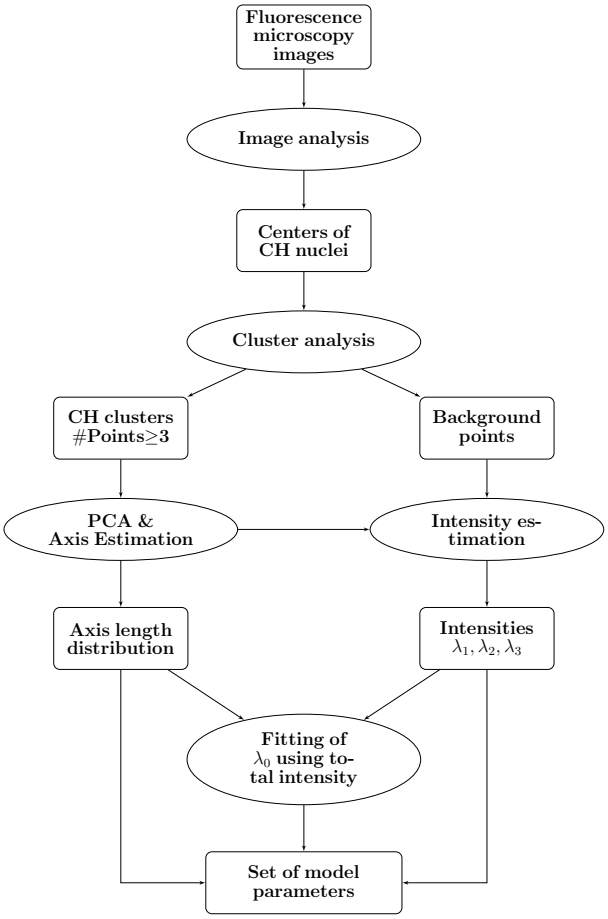

Figure 6: Fitting of the point process model to microscopy data.

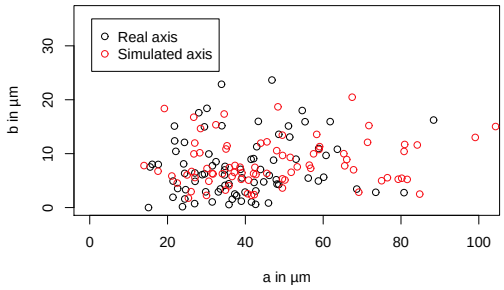

Figure 7: Semi-axis lengths of ellipses as found in the data (black points) and the simulations (red points), by random selection of 80 ellipses. The two coordinates depict the lengths of the major and minor semi-axes, respectively. The semi-axis lengths of the simulated data have been obtained by sampling from a single model realization on a large sampling window.

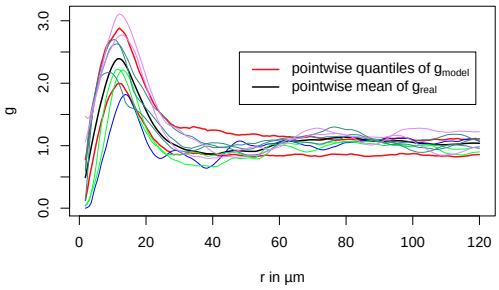

(a) Pair-correlation function

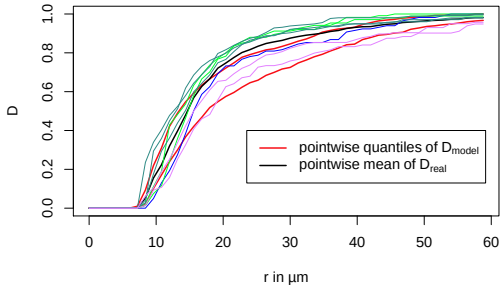

(b) Nearest neighbor distance distribution function

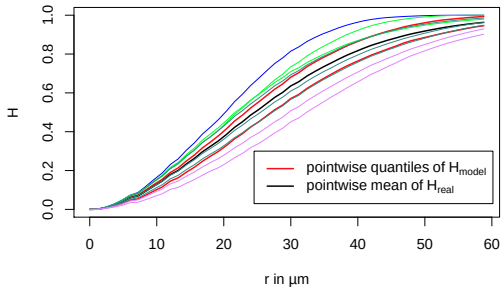

(c) Spherical contact distribution function

Figure 8: Comparison of empirical point pattern characteristics between 8 microscopy images of the articular cartilage surface in the human knee joint and simulations. Red lines depict 90% envelope curves of the model, the black line is the pointwise mean of the estimators for real data. The other lines correspond to single images, where colors specify different subjects, (subject 1 $\widehat{=}$ blue, subject 2 $\widehat{=}$ green, subject 3 $\widehat{=}$ turquoise, subject 4 $\widehat{=}$ violet).